

1 A Fast Method for Detecting Rock Blocks and Calculating Volumes 2 and 3D Surface Areas

3 Ali Polat

4 Provincial Directorate of Disaster and Emergency, 58000, Sivas, Turkey

5 ARTICLE INFO

6
7 **Keywords:**
8 Rock segmentation
9 U-Net
10 Convolutional Neural Networks
11 Rockfall
12 Volume Calculation
13 3D Surface Area Calculation

ABSTRACT

14 Rockfall events are a type of natural disaster that causes loss of life and property in the world.
15 The risk of rockfall can be eliminated by using rockfall prevention methods. To choose the most
16 suitable method, projecting studies should be carried out. This study aims to automatically detect
17 rock blocks in a region and calculate their volumes and 3D surface areas. For this purpose, U-Net
18 segmentation method and Python software language were used. DenseNet121 transfer learning
19 method based on convolutional neural networks was used for feature extraction. The data set
20 was created from the orthophoto images obtained by an unmanned aerial vehicle (UAV). Using
21 the random sampling method, 369 images were selected for training and 191 images for test.
22 As a result of the analysis, the mean IOU (Intersection Over Union) was calculated as 85% for
23 training and 84% for test. The trained model was applied to the study area and 3111 rock blocks
24 were detected. The resulting map is saved as a vector file with coordinates and can be opened
25 in any GIS software. The volumes and 3D surface areas of the rock blocks were calculated with
26 Python software as 275.93 m³ and 2615.23 m², respectively. With this study, rock blocks can be
detected automatically, and their volumes and 3D surface areas can be measured. These results
can be used in the selection of rockfall prevention methods. In addition, the codes used in this
study can automatically detect different geological formations from aerial photographs. Also,
volume and 3D surface area algorithms developed in this study can be used to calculate different
types of objects.

27

28 1. Introduction

29 In many parts of the world, loss of life and property is experienced, and large-scale economic losses occur due to
30 natural disasters. One of these natural disasters is rockfall events. Rockfalls are a type of slope instability in which
31 blocks of rock confined to discontinuities move very rapidly from the source region (Varnes, 1978; Hutchinson, 1988;
32 Cruden and Varnes, 1996). Due to the high velocity during the event, rockfalls can be very dangerous for structures in
33 their route depending on the block size. Although it is a type of disaster that affects small areas, its consequences can
34 be very serious. That's why rockfall prevention studies are important. There are studies on this subject in the literature
35 (Liu et al., 2021; Keskin and Polat, 2022; Ji et al., 2023; Kainthola et al., 2023; Cao et al., 2024). Some preliminary
36 studies are needed to develop a prevention method. One of them is the detection of rock blocks and the calculation of
37 their geometric properties. In this study, rock blocks were segmented, and their volumes and 3D surface areas were
38 calculated.

39 There are various studies on rock segmentation in the literature. Dunlop (2006) developed a technique for the
40 characterization of rocks using albedo, color, texture, and shape features. In that work, rocks in natural scenes were
41 segmented and located with accurate boundaries. For segmentation purpose top-down and bottom-up knowledge are

ORCID(s): 0000-0002-9147-3633 (A. Polat)

42 combined, and geologic rock analysis performed successfully.

43 In the study conducted by Song and Shan (2006) in 2006, rock segmentation on Mars was performed to plan
44 routes and determine landing areas. Texture-based image segmentation and edge-flow driven active contour has been
45 developed. Wavelet based local transform, multi-resolution histograms, and inter-scale decision were combined and
46 used for rock segmentation. As a result of the experiments, Song and Shan (2006) obtained reliable rock segmentation
47 results.

48 The place of visual navigation in planetary rover autonomy is crucial. Rock segmentation is an important and
49 challenging task for rover autonomy due to the high computational load and real-time requirement. Kuang et al.
50 (2021) propose a rock segmentation network (NI-U-Net++) to aid in the visual navigation of rovers. The created
51 model consists of two steps. In the first step, called pre-training, synthetic rock images are generated and used to
52 pre-train the NI-U-Net++ network. In the second phase, transfer-training, the pre-trained NI-U-Net++ network is
53 fine-tuned using real-life images.

54 Guo et al. (2022) proposed an adaptive watershed segmentation method based on distance transformation for blasted
55 rock piles images. They obtained 95.65% segmentation accuracy for limestone and granite rock blocks with area over
56 100 cm².

57 Segmentation of rocks is important in mining as well as in geology. Segmentation is used in this area to determine
58 the size distribution of rock fragments, to organize and optimize blasting, and to reduce environmental impact. For this
59 purpose, Malladi et al. (2014) proposed a simple superpixel algorithm called Superpixels Using Morphology (SUM),
60 which uses a watershed transformation approach to generate superpixels; and made a study comparing some of the
61 current superpixel algorithms on rock images.

62 Recently, various deep learning and machine learning algorithms, including Convolutional Neural Networks (CNN),
63 have been proposed by researchers working on rock segmentation. Karimpouli and Tahmasebi (2019) used convolutional
64 autoencoder networks called SegNet for segmentation of digital rock images. Due to the limited number of rock
65 images, cross-correlation based simulation was applied to increase the number of images. 20 images taken from Berea
66 sandstone were used as dataset. As a result of the experiments, they obtained an accuracy value of 96%.

67 Xue et al. (2021) made rock segmentation study for a different purpose; they proposed the rock segmentation
68 visual system to assist Tunnel Boring Machine (TBM) driving. TBM is an essential equipment for digging long-range
69 tunnels. They applied different deep learning network for semantic segmentation of rocks.

70 In the above studies, rock segmentation was carried out for different purposes. In this study, rock segmentation
71 was carried out as a necessary preliminary study in the development of rockfall prevention methods. Rock blocks
72 were detected precisely in a fast, economical, and safe manner. In addition, the volumes and 3D surface areas of rock
73 blocks were calculated. The methods and algorithms used in the study can be used in many fields such as engineering

74 applications, and geological-geomorphological studies.

75 **1.1. Study area**

76 The study area is in the north of Karasar village, which is approximately 156 km away from Sivas city (Fig. 1).
 77 This area consists of Middle Miocene aged agglomerate and tuff units (MTA 1/25000) (Fig. 2). This unit was defined
 78 as Adatepe volcanites according to Yilmaz and Yilmaz (2004). The unit consists of black, red-brown, and brown-
 79 black colored basaltic lava flows and less commonly agglomerate and tuffs. The rock blocks in this unit expose a risk
 80 of rockfall. Lower Miocene aged sandstone-mudstone-limestone units are observed in the settlement area (Karasar
 81 village) and vicinity.

82 Karasar village is located on the slopes of a hill. The bedrock on the hill is heavily fractured and cracked. There are
 83 many rock blocks that have fallen from the upper parts of the slope. The sizes of these blocks vary from 0.5 m³ to 15
 84 m³. Rapid temperature changes, heavy snow and precipitation, freeze-thaw cycles, earthquakes, and human-induced
 85 factors increase the risk of rockfall in the region.

86 **2. Methodology**

87 Creating the dataset is a big problem for classification or segmentation processes. In this study, Unmanned Air
 88 Vehicle (UAV) was used to collect data. An orthophoto image of the region was created from aerial photographs
 89 obtained by UAV. Model building processes were conducted in a part of the study area. Training and testing images
 90 were generated from this region. Rock blocks were labeled, and mask images were created. The segmentation process
 91 was then carried out using Python and necessary libraries, and the results were converted into polygon vector files.
 92 Additionally, the volumes and 3D surface areas of all the rocks were calculated (Fig. 3).

93 **2.1. Data preparation**

94 In this study required data was collected by UAV. DJI phantom 3-Pro was used for image acquisition. First, the
 95 area to be flown is determined, then the necessary parameters for image acquisition are entered by the Pix4d Capture
 96 software. These parameters were chosen as follows.

- 97 – Flight altitude (altitude): 100 m.
 98 – Flight speed (speed): Fast
 99 – Camera angle (Angle): 70°
 100 – Overlap: 80%

101

102 The flight was carried out by the "Double Grid" method. The model of UAV used in this study does not have an
 103 obstacle detecting feature. Therefore, when determining the height, it is necessary to pay attention to the nearby power

104 lines, tall buildings, trees, and peaks of hills.

105 The camera model (FC00X) of UAV has 4000×3000 resolution, 3.61 mm focal length and 1.56×1.56 μm pixel

106 dimensions. After the flight, 284 images were obtained, and these images were processed with the Pix4Dmapper

107 software. As a result, an orthophoto image with a resolution of 3.51 cm/pixel and a dimension of 2329×1587 was

108 created.

109 A region was selected from a large orthophoto image to create training and testing images. This area was chosen

110 randomly. All visible rocks in the image were outlined using GIS software. The resulting file was saved as a vector

111 file and used as mask data in the segmentation process. Following this, image and mask files were created separately.

112 A deep learning model requires the same-sized images. That's why a single image needs to be split into patches.

113 The patch dimension was used as 256×256. Train-test splitting rate was selected as 66% for training data and 34% for

114 testing data. The large image was split into 9 parts to avoid sampling from the same regions. Areas 1,5, and 9 were

115 selected for creating test images. Train images were selected from the other (2,3,4,6,7,8) areas (Fig. 4). A total of

116 560 images (256×256) were selected, 369 images for training and 191 images for testing. The same processes were

117 applied to extract the mask images.

118 The Albumentations (Buslaev et al., 2020) method was also used for data augmentation during the model-building

119 stage. Albumentations includes many transform methods. The augmentation methods listed below were applied:

- 120 – horizontal flip
- 121 – affine transforms
- 122 – perspective transforms
- 123 – brightness/contrast/colours manipulations
- 124 – image blurring and sharpening
- 125 – gaussian noise

126

127 2.2. Model building

128 In this study, U-Net architecture (Ronneberger et al., 2015) was used as segmentation model. This architecture is

129 a type of fully convolutional network developed for biomedical image segmentation. It is named U-Net because the

130 shape of the architecture is like the letter U. The network architecture of U-Net is shown in Fig. 5. It consists of two

131 parts: contracting path (left side) and expanding path (right side). The first part captures context, and the second part

132 enables precise localization. The left side consists of four blocks and each block contains two 3×3 convolution layers

133 + activation function (with batch normalization) and one 2×2 max-pooling layer. Also, the right side consists of four

134 blocks. These blocks include the steps of deconvolution layer, merging with feature map from subsampling path, 3×3

135 convolution layer + activation function (with batch normalization). Finally, an additional 1×1 convolution operation
 136 is applied to reduce the feature map to the required number of channels and generate the segmented image.

137 DenseNet121 transfer learning model was used for feature extraction and rock segmentation was performed with
 138 U-Net. Segmentation model was evaluated in terms of IoU and F1-score metrics. IoU, which is frequently preferred in
 139 segmentation problems, is also known as the Jaccard similarity coefficient (Jaccard, 1912). It is the ratio of correctly
 140 classified pixels to the sum of the number of pixels in that class and the predicted number of pixels (Equation 1).

$$J(A, B) = \frac{|A \cap B|}{|A \cup B|} \quad (1)$$

141 The F1-Score is important in that it is not False Negative or False Positive, but a measurement metric that includes all
 142 error costs. It is the harmonic mean of Precision and Recall values (Equation 2).

$$F1\text{-}Score = \frac{2 \times \text{Precision} \times \text{Recall}}{\text{Precision} + \text{Recall}} \quad (2)$$

$$\text{Precision} = \frac{TP}{TP + FP}$$

$$\text{Recall} = \frac{TP}{TP + FN}$$

143 Where TP is True Positive, FP is False Positive and FN is False Negative.

144 3. Results

145 In this study, we created our own dataset. A large orthophoto image with a dimension of 2329×1587 was created
 146 from UAV images. This image needs to be patched for use in the segmentation model. A python script has been written
 147 for this purpose. It is possible to create the desired number and size of images with the written script. Random corner
 148 coordinates with the size of 256×256 patches were created. Obtaining images with the exact corner coordinates was
 149 prevented. Because of this condition, the program gives an error when too many images are wanted to be created.

150 Also, the probability of creating very similar images increases. Using the grid method, 56 images can be obtained
 151 from the large orthophoto image. Using the random sampling method 560 images were obtained from the same image.

152 U-Net segmentation model was used with DenseNet121. IOU and F1-score were used as performance metrics.
 153 The model was trained and tested with different parameters. The parameters providing the best results are given in
 154 Table 1 below.

155 IoU scores and losses graph of model are shown in Figure 6. The results of the model are satisfactory for the

Table 1
Model parameters

Optimizer	Adam
Learning rate	0.0001
Batch size	8
Image size	256×256
Epoch	100

156 segmentation task. Train IoU, test IoU, train F1-score and test F1-score were calculated as 0.85%, 0.85%, 0.92%, and
157 0.92%, respectively.

158 The trained model successfully detected rock blocks within the study area (Fig. 7). The boundaries of 3111 rocks
159 of various sizes were determined and created as a vector file (.shp). This method is not recommended for smaller areas.
160 Because sufficient training data cannot be created. In areas where there are several rock blocks, detection can also be
161 done manually. Sometimes there may be distortions at the edges and corners of the image. This causes errors in rock
162 block detection. Therefore, a larger area than the area where the rocks are located should be selected as the study area.

163 After the rocks were detected, each rock's volume and 3D surface area were calculated. These calculations were
164 performed using Python. Calculated values were saved in the shape file as fill volume, cut volume and 3D area.

165 In volume calculations, there must be a reference height or surface. In this study, the heights at the boundaries of
166 the rocks were selected as the reference height. The calculations were made using an image containing elevation data.
167 This image consists of pixels containing elevation values, which are organized into rows and columns. The elevation
168 values in each row were used to calculate the total volume. The polygons showing the boundaries of the rocks were
169 masked with elevation data. Thus, data with elevation values for each rock were obtained. Volumes were calculated
170 by proceeding along the rows. The slope was calculated by comparing the elevation values at the beginning and end
171 of the row. A new base elevation was determined for each pixel and the volumes were calculated from this elevation.

172 In this method, it is necessary to evaluate three different scenarios. In the first case, the first and last elevations of
173 the rows are equal. Here, the starting elevation value is used as the reference height. Volumes above this elevation are
174 calculated as fill volumes, while volumes below are calculated as cut volumes. In the second case, the first elevation
175 is greater than the last elevation of the rows. In the third case, the first elevation is less than the last elevation of the
176 rows. Different calculations are required for each scenario. These situations are illustrated in Figure 8.

177 Volume calculation can be easily done by multiplying the pixel area by the height. Heights need to be calculated
178 for each pixel. The starting and ending pixels along a row are assumed to be ground. These ground elevations are used
179 to find the slope, and each pixel's height is recalculated using this slope. Fill volume and cut volume were calculated
180 using new heights and pixel areas. Slopes, fill volumes and cut volumes were determined using the method in Figure
181 8. The total volumes (fill and cut) are found by summing the calculations made for each row.

182 The 3D surface area was calculated by Python script. Calculations of flat surfaces can be found by multiplying
 183 pixel lengths. However, different methods must be used for irregular surfaces. The gradient method was used in 3D
 184 surface calculation. Height changes were calculated in X and Y directions, gradient vectors were obtained in each
 185 direction. Surface areas were calculated by using these vectors. The slope correction equation is used to determine the
 186 sloped surfaces (Equation 3).

$$\text{slope correction} = \sqrt{1 + \left(\frac{\partial z}{\partial x}\right)^2 + \left(\frac{\partial z}{\partial y}\right)^2} \quad (3)$$

$$\frac{\partial z}{\partial x} = \text{gradient in X direction}, \quad \frac{\partial z}{\partial y} = \text{gradient in Y direction} \quad (4)$$

The 3D surface area is calculated as following:

$$\text{3D surface area} = \text{pixel area} \times \text{slope correction} \quad (5)$$

187 4. Conclusions

188 This study aims to segment rock blocks and calculate the volume and 3D surface areas of the blocks obtained as a
 189 result of segmentation. The methods used in the segmentation process provided the determination of the boundaries
 190 of rock blocks with high accuracy rates. In this way, the geometric properties of the blocks were analysed in detail.

191 U-Net deep learning network and DenseNet121 model were used as segmentation methods. The boundaries of
 192 rock blocks were determined accurately with the trained model.

193 The volume of each rock block was successfully calculated from the data obtained after segmentation. Similarly,
 194 the 3D surface areas of the blocks were calculated. High-resolution Digital Elevation Map (DEM) data were used in
 195 volume and surface area calculations. Determination of block volumes and 3D surface areas is of critical importance,
 196 especially for rockfall simulations and engineering analyses. In addition, since the outputs of the study are coordinated
 197 vector data, they can be easily used in any GIS software. It can be a basis for different studies and analyses.

198 This study has presented a reliable method for segmentation and volume/surface area calculations and has also
 199 directly contributed to engineering applications in terms of determining the physical properties of rock masses. The
 200 segmentation section of the study is recommended for terrains containing a lot of rock blocks. It is possible to detect
 201 rock blocks in a short time. In addition, this method can be used to automatically detect different types of terrain. Deep

202 learning models usually require a large amount of data for training. A large amount of data can be generated with the
203 Random Sampling method proposed in this study. Volume and 3D surface area algorithms can be used not only for
204 rock blocks but also for any object on the field. These algorithms only require precise DEM data and object boundaries.
205 For example, these calculations can be made for a single rock block. In these calculations, ground heights and object
206 heights must be determined clearly. When determining the object boundaries, they should be extended towards the
207 ground. If the boundaries only represent the object, the ground heights will not be considered, and the results will not
208 be correct. In some cases, the model can draw the boundaries of the rock blocks narrower. In this case, this problem
209 can be solved by adding buffers to the rock blocks.

210 As a result, this study provides a basis for volumetric and geometric analyses for rock mechanics, geology and
211 engineering applications, and can be expanded by testing on different rock types and fields in future studies.

212 **5. Acknowledgments**

213 The author wants to thank the Prime Ministry Disaster and Emergency Management Authority for supplying or-
214 thophoto images and geological map.

215 **Code availability section**

216 Name of the code: rock_segmentation

217 Contact: ali.polat@afad.gov.tr

218 Program language: Python

219 Software required: Python v3.9

220 Program size: 35.7 KB

221 The source codes are available for downloading at the link: https://github.com/apolat2018/rock_segmentation222 **References**

- 223 Buslaev, A., Iglovikov, V.I., Khvedchenya, E., Parinov, A., Druzhinin, M., Kalinin, A.A., 2020. Albumentations: fast and flexible image augmen-
224 tations. *Information* 11, 125.
- 225 Cao, Z., Liu, Z., Xu, G., Lin, H., Li, X., Nikitas, N., 2024. Risk assessment and prevention for typical railway bridge pier under rockfall impact, in:
226 *Structures*, Elsevier. p. 106178.
- 227 Cruden, D.M., Varnes, D.J., 1996. Landslide types and processes. *Transportation Research Board, US National Academy of Sciences, Special*
228 *Report 247*, 36–75.
- 229 Dunlop, H., 2006. Automatic rock detection and classification in natural scenes. *Masters Thesis, Carnegie Mellon University* .
- 230 Guo, Q., Wang, Y., Yang, S., Xiang, Z., 2022. A method of blasted rock image segmentation based on improved watershed algorithm. *Scientific*
231 *Reports* 12, 7143.
- 232 Hutchinson, J., 1988. Morphological and geotechnical parameters of landslides in relation to geology and hydrogeology, landslides, in: *Proceedings*
233 *of the fifth international symposium on landslides*, pp. 3–35.
- 234 Jaccard, P., 1912. The distribution of the flora in the alpine zone. 1. *New phytologist* 11, 37–50.
- 235 Ji, Z.M., Chen, T.L., Wu, F.Q., Li, Z.H., Niu, Q.H., Wang, K.Y., 2023. Assessment and prevention on the potential rockfall hazard of high-steep
236 rock slope: a case study of zhongyuntai mountain in lianyungang, china. *Natural Hazards* 115, 2117–2139.
- 237 Kainthola, A., Pandey, V.H.R., Singh, P., Singh, T., 2023. Stability assessment of markundi hills using q-slope, smr and simulation tools, in:
238 *Landslides: Detection, Prediction and Monitoring: Technological Developments*. Springer, pp. 87–107.
- 239 Karimpouli, S., Tahmasebi, P., 2019. Segmentation of digital rock images using deep convolutional autoencoder networks. *Computers & geosciences*
240 126, 142–150.
- 241 Keskin, İ., Polat, A., 2022. Kinematic analysis and rockfall assessment of rock slope at the unesco world heritage city (safranbolu/turkey). *Iranian*
242 *Journal of Science and Technology, Transactions of Civil Engineering* 46, 367–384.
- 243 Kuang, B., Wisniewski, M., Rana, Z.A., Zhao, Y., 2021. Rock segmentation in the navigation vision of the planetary rovers. *Mathematics* 9, 3048.
- 244 Liu, W.l., Dong, J.x., Xu, H.h., Sui, S.g., Yang, R.x., Zhou, L.s., 2021. Trajectory analysis and risk evaluation of dangerous rock mass instability of
245 an overhang slope, southwest of china. *Advances in civil engineering* 2021, 7153535.
- 246 Malladi, S.R.S., Ram, S., Rodríguez, J.J., 2014. Superpixels using morphology for rock image segmentation, in: *2014 Southwest Symposium on*
247 *Image Analysis and Interpretation*, IEEE. pp. 145–148.
- 248 Ronneberger, O., Fischer, P., Brox, T., 2015. U-net: Convolutional networks for biomedical image segmentation, in: *Medical image computing and*
249 *computer-assisted intervention–MICCAI 2015: 18th international conference, Munich, Germany, October 5–9, 2015, proceedings, part III* 18,
250 Springer. pp. 234–241.

Short title

- 251 Song, Y., Shan, J., 2006. A framework for automated rock segmentation of the mars exploration rover imagery. URL: <https://api.semanticscholar.org/CorpusID:39798752>.
- 252
- 253 Varnes, D., 1978. Slope movement types and processes. *Landslides: analysis and control* .
- 254 Xue, Z., Chen, L., Liu, Z., Lin, F., Mao, W., 2021. Rock segmentation visual system for assisting driving in tbm construction. *Machine Vision and*
- 255 *Applications* 32, 77.
- 256 Yılmaz, H., Yılmaz, A., 2004. Divriği (sivas) yöresinin jeolojisi ve yapısal evrimi. *Türkiye Jeoloji Bülteni* 47, 13–46.

257 **List of Figures**

258 1	Location map	12
259 2	Geological map (1/25000 scale geological map of General Directorate of Mineral Research and Ex- 260 plorations) (a), rock blocks (b), settlement and rocks (c)	13
261 3	Workflow diagram	14
262 4	Train and test sampling areas. 1,5,9 test sampling area and 2,3,4,6,7,8 train sampling area	15
263 5	U-Net architecture	16
264 6	DenseNet121 IoU and Loss values	17
265 7	Result map of the model (a) original view, (b,c,d)zoomed views.	18
266 8	Volume calculation methods. (a) first height is greater than the last height of the rows,(b) b) first height 267 is less than the last height of the rows	19

Short title

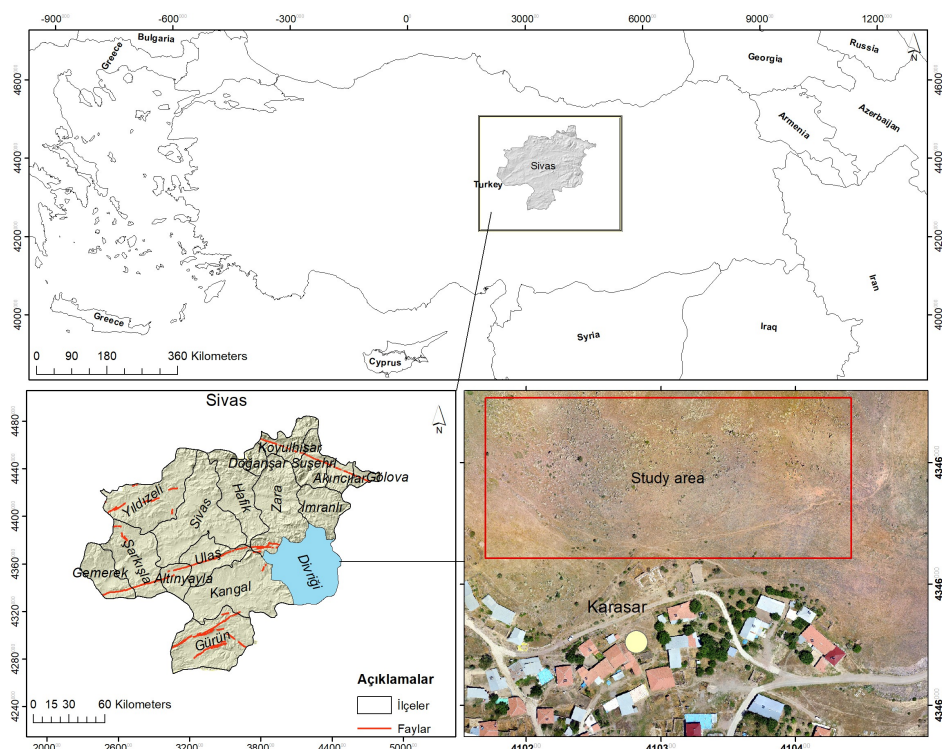
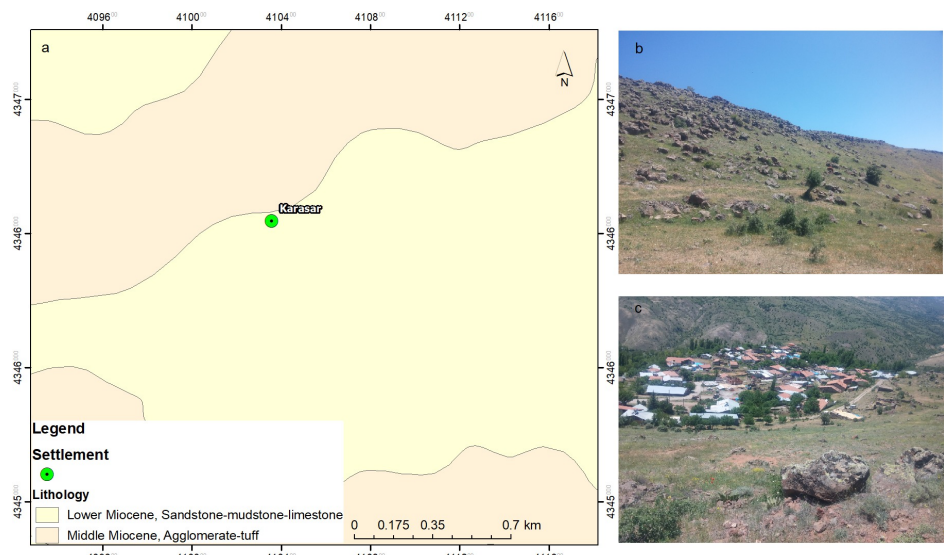


Figure 1: Location map



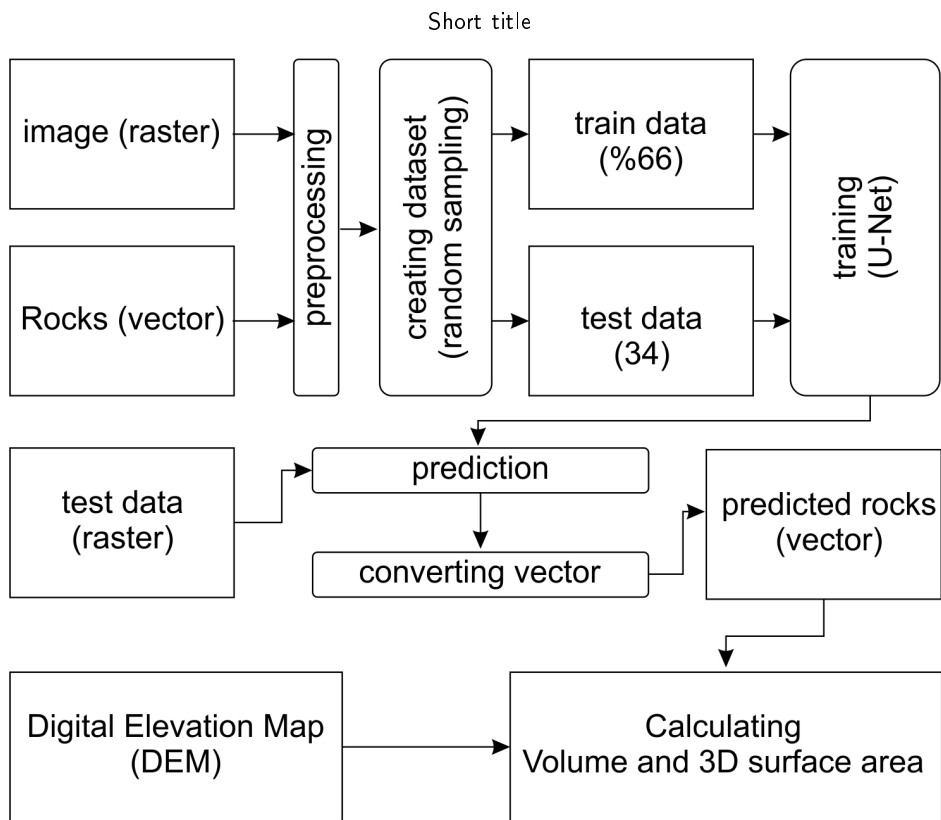


Figure 3: Workflow diagram

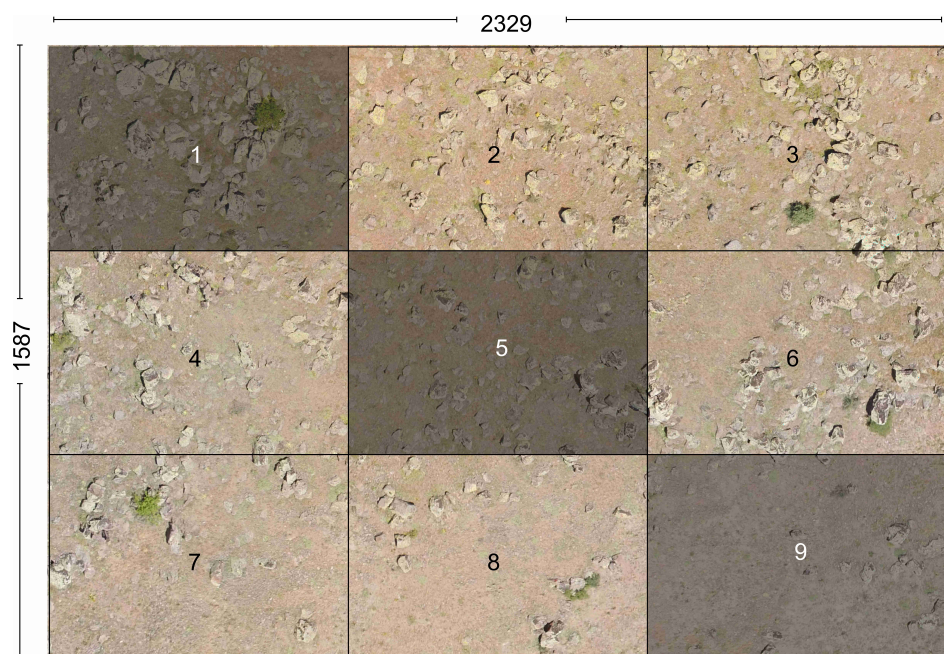
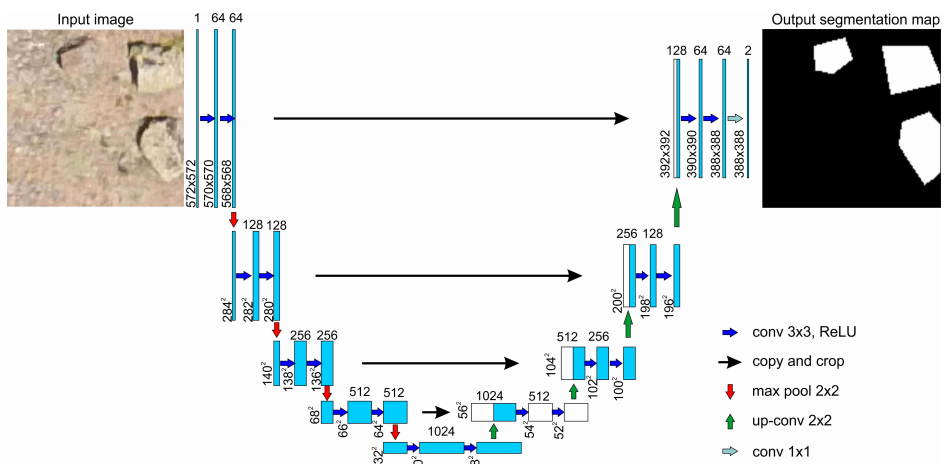


Figure 4: Train and test sampling areas. 1,5,9 test sampling area and 2,3,4,6,7,8 train sampling area

**Figure 5:** U-Net architecture

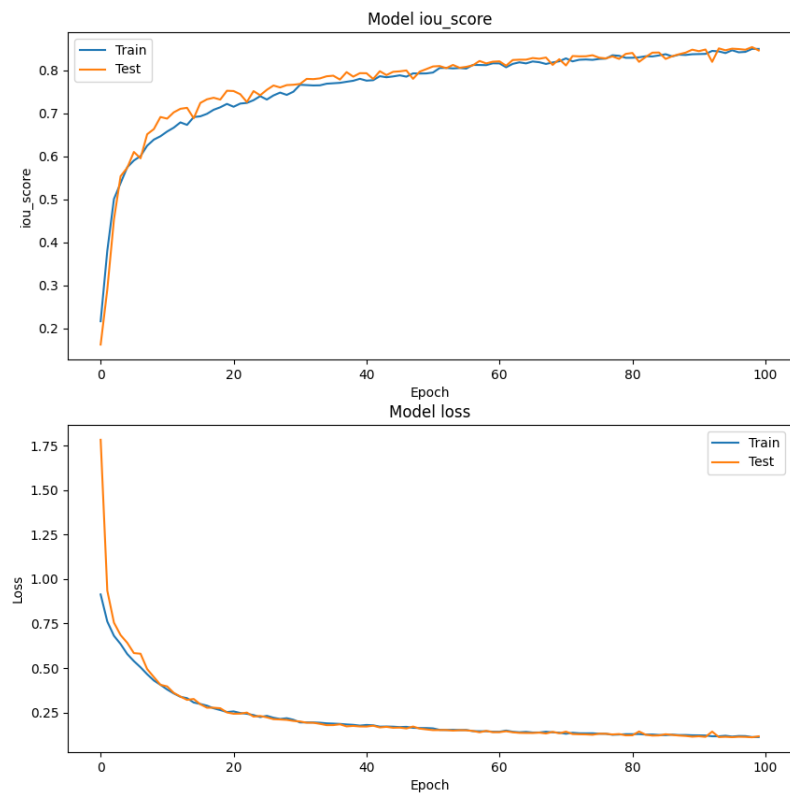


Figure 6: DenseNet121 IoU and Loss values

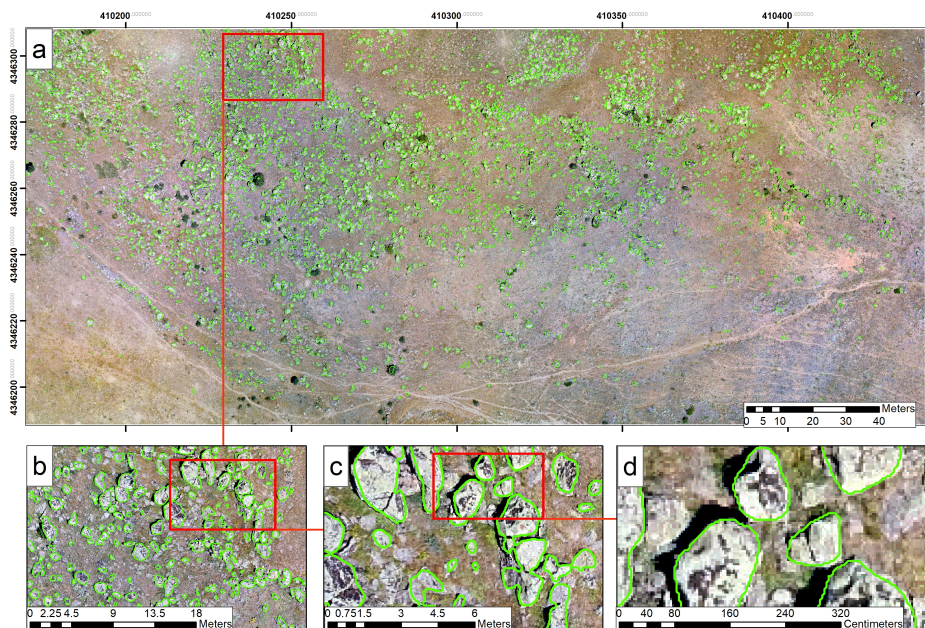


Figure 7: Result map of the model (a) original view, (b,c,d)zoomed views.

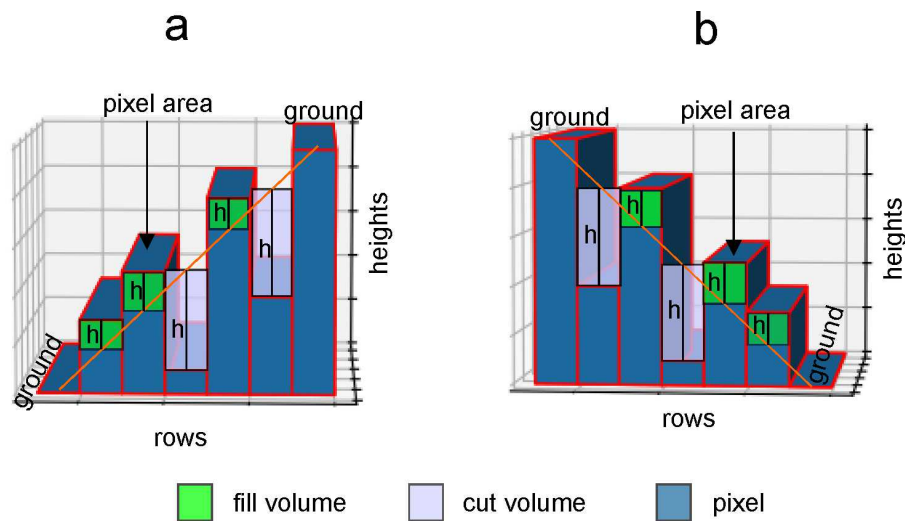


Figure 8: Volume calculation methods. (a) first height is greater than the last height of the rows,(b) b) first height is less than the last height of the rows